Nonradial and nonpolytropic astrophysical outflows

VI. Overpressured winds and jets

C. Sauty[1], E. Trussoni[2], and K. Tsinganos[3]

[1] Université Paris 7, Fédération APC - Observatoire de Paris, LUTH, 92190 Meudon, France
[2] Istituto Nazionale di Astrofisica (INAF) – Osservatorio Astronomico di Torino, Strada Osservatorio 20, 10025 Pino Torinese (TO), Italy
[3] IASA and Section of Astrophysics, Astronomy & Mechanics Department of Physics, University of Athens, Panepistimiopolis 157 84, Zografos, Greece

Abstract. By means of a nonlinear separation of the variables in the governing full set of the magnetohydrodynamic (MHD) equations for axisymmetric plasmas we analyse an exact model for magnetized and rotating outflows that are hotter and overpressured at their axis. These outflows start subsonically and subAlfvénically from the central gravitating source and its surrounding accretion disk. Subsequently they accelerate thermally and magnetocentrifugally and thus cross the appropriate MHD critical points, reaching high values of the Alfvén Mach number. Three types of solutions are found: (a) collimated jet-type outflows from efficient magnetic rotators with the flow confined by the magnetic hoop stress; (b) radially expanding wind-type outflows analogous to the solar wind, from inefficient magnetic rotators or strongly overpressured sources; (c) terminated solutions with increasing amplitude of oscillations in the width of the beam. In contrast to previously studied underpressured outflows, the transition from collimated jets to uncollimated winds is not continuous in the appropriate parametric space with a gap where no stationary solution is found. Superfast at infinity solutions are filtered by three critical points corresponding to the three known limiting characteristics or separatrices of MHD wind theory. Collimated and terminated solutions cross the slow, Alfvén and fast magneto-acoustic critical points. Radially expanding solutions cross the slow and Alfvén critical points while the last boundary condition is imposed by requiring that the pressure vanishes at infinity.

Key words. magnetohydrodynamics (MHD) – Sun: solar wind – stars: pre-main sequence – stars: winds, outflows – ISM: jets and outflows – galaxies: jets

1. Introduction

One well known example that demonstrate analytically that astrophysical jets can be accelerated and collimated magnetically is the Blandford & Payne 1982 model. This model has been shown to be the prototype of the wide family of the so-called *radially* self-similar disk wind-type outflows, recently reexamined analytically and numerically (e.g., Ouyed & Pudritz 1997; Vlahakis & Tsinganos 1998; Krasnopolsky et al. 1999; Casse & Ferreira 2000; Ustyugova et al. 2000; Krasnopolsky et al. 2003; Kudoh et al. 2002; Casse & Keppens 2004).

A complementary wide class of MHD outflow solutions, which quantitatively demonstrated the transition of collimated outflows from efficient magnetic rotators to uncollimated outflows from less efficient magnetic rotators, is self-similar in the *meridional* direction (see Sauty et al. 2002a; henceforth STT02, and references therein). This class of models may describe ordinary stellar winds, or collimated outflows composed of a central jet core surrounded by a disk wind (Tsinganos & Bogovalov 2002). Although this model is somewhat similar in geometry to an X-wind (e.g., Shu et al. 1994; Shang et al. 2002), it nevertheless has some differences, such as it consistently solves the full set of the MHD equations from the source to the far region and also that the connection between the disk and the magnetosphere is an X point rather than a fan of concentrated magnetic flux. This class of analytical models may also be compared to the corresponding relaxation states of recent numerical simulations (e.g., Koide et al. 1998; Bogovalov & Tsinganos 1999; Keppens & Goedbloed 2000; Matt et al. 2003; Koide et al. 2000; Koide 2003) as is discussed in Sect. 6.2.

In such meridionally self-similar models, one may either prescribe the poloidal structure of the streamlines, or assume a relationship between the radial and longitudinal components of the gas pressure gradient. The main properties of the first class of solutions which are asymptotically collimated are outlined in Trussoni et al. (1997; henceforth TTS97) wherein the essential role of rotation in getting cylindrical collimation has

been demonstrated. On the other hand, if the two components of the pressure gradient are related, the meridional structure of the streamlines is self-consistently deduced from the solution of the full set of the MHD equations. Such rotating and magnetized outflows with a spherically symmetric structure of the gas pressure may be asymptotically superAlfvénic with radial or collimated fieldlines, depending on the efficiency of the magnetic rotator (Sauty & Tsinganos 1994; henceforth ST94).

In Sauty et al. (1999; henceforth STT99) we extended the results of ST94 by performing an asymptotic analysis of the meridionally self-similar solutions for a non spherically symmetric structure of the pressure. It was pointed out there that a superAlfvénic outflow may encounter different asymptotic conditions where it can be thermally or magnetically confined, and thermally or centrifugally supported.

Current-carrying *underpressured* flows with a pressure increasing as we move away from the axis, were studied in STT02. They were found to be either thermally or magnetically cylindrically collimated around their axis, depending on whether the efficiency of the magnetic rotator prevails or not to the thermal confinement, respectively. They have been shown to be well suited to describe various astrophysical winds and jets (see Lima et al. 2001; Meliani 2001; Sauty et al. 2003).

We complete here this work by studying *overpressured* outflows, i.e., with a pressure decreasing away from the system axis. Such outflows can only be collimated via magnetic stresses if the magnetic rotator is sufficiently efficient. Otherwise the flow structure attains asymptotically a radial configuration. We present complete solutions that connect the base of the flow with its superAlfvénic regime. In particular we investigate if, and under which conditions, the basal region can be matched to the asymptotic solutions outlined in STT99. Conversely to the previous study reported in STT02, the present analysis requires a very careful topological study of the MHD self-similar equations because of the presence of a second X-type magnetosonic critical point.

In the following Sect. 2 and in order to establish the used notation we briefly review the assumptions, parameters, variables and mathematical structure of the present model. In Sect. 3 the asymptotic behaviour of the solutions presented in STT99 is also very briefly outlined. The results and parametric study are presented in Sect. 4 while the main properties of the three classes of cylindrical, radial and terminated solutions are summarized in Sect. 5. Finally, in Sect. 6 we discuss the astrophysical relevance of our results, in particular in relation to jets associated with young stellar objects.

2. Governing equations for meridional self-similar outflows

We summarize here the main assumptions of our meridionally ($\theta-$) self-similar treatment of the MHD equations. More details can be found in STT94, STT99 and STT02.

2.1. Summary of the basic assumptions

The basic equations governing plasma outflows in the framework of ideal MHD are the momentum, mass and magnetic flux conservation equations, together with the frozen-in law for infinite conductivity and the first law of thermodynamics. First, with axisymmetry the poloidal component of the magnetic field can be derived from a magnetic flux function $A(r, \theta)$ in spherical coordinates (r, θ, φ),

$$\boldsymbol{B} = \frac{\boldsymbol{\nabla} A}{r \sin \theta} \times \hat{\varphi}. \tag{1}$$

Next, for steady flows, we judiciously specify the meridional dependences of the velocity and magnetic fields, as well as of the density and pressure, V, $\boldsymbol{B}$, P and ρ respectively, which may be written as follows (for details see ST94, STT99 and STT02):

$$B_r = \frac{B_*}{G^2(R)} \cos \theta, \tag{2}$$

$$B_\theta = -\frac{B_*}{G^2(R)} \frac{F(R)}{2} \sin \theta, \tag{3}$$

$$B_\varphi = -\frac{\lambda B_*}{G^2(R)} \frac{1 - G^2(R)}{1 - M^2(R)} R \sin \theta, \tag{4}$$

$$V_r = V_* \frac{M^2(R)}{G^2(R)} \frac{\cos \theta}{\sqrt{1 + \delta \alpha(R, \theta)}}, \tag{5}$$

$$V_\theta = -V_* \frac{M^2(R)}{G^2(R)} \frac{F(R)}{2} \frac{\sin \theta}{\sqrt{1 + \delta \alpha(R, \theta)}}, \tag{6}$$

$$V_\varphi = \frac{\lambda V_*}{G^2(R)} \frac{G^2(R) - M^2(R)}{1 - M^2(R)} \frac{R \sin \theta}{\sqrt{1 + \delta \alpha(R, \theta)}}, \tag{7}$$

$$\rho(R, \alpha) = \frac{\rho_*}{M^2(R)} (1 + \delta \alpha), \tag{8}$$

$$P(R, \alpha) = \frac{1}{2} \rho_* V_*^2 \Pi(R)[1 + \kappa \alpha] + P_0. \tag{9}$$

In the above definitions, κ, λ, δ and P_0 are model parameters while we have also used the dimensionless magnetic flux function $\alpha(R, \theta) = 2 A(r, \theta)/r_*^2 B_*$. Note that conversely to STT99 and papers before, we use a more flexible definition of the pressure function, as in STT02. The dimensionless pressure along the polar axis is defined as $\Pi(R)$ within some free additive constant P_0. It does not appear in the final dynamical equations as they depend only on the pressure gradient. However, this constant can be adapted to the boundary conditions. In radial solutions where Π goes asymptotically to zero, P_0 should also vanish to ensure that the temperature does not diverge as the mass density also goes asymptotically to zero. Conversely, in cylindrically collimated flows where Π can be a negative function, P_0 should be adjusted such that the total pressure remains everywhere positive.

The square of the poloidal Alfvén number

$$M^2 \equiv M^2(r) = 4\pi\rho \frac{V_p^2}{B_p^2}, \tag{10}$$

is assumed to be solely a function of the radial distance. For convenience we have normalized all quantities at the Alfvén surface along the rotation axis, $r = r_*$. The dimensionless radial distance is denoted by $R = r/r_*$, while B_*, V_* and ρ_* are the

poloidal magnetic field, velocity and density along the polar axis at the Alfvén radius r_*, with $V_*^2 = B_*^2/4\pi\rho_*$.

A second assumption is that the cylindrical distance $\varpi(R, \alpha)$ of a poloidal fieldline from the axis is separable in the variables R and α, as $\varpi^2 = G^2(R)\alpha$, where $G^2(R)$ is the cross sectional area of a flux tube perpendicular to the symmetry axis, in units of the corresponding area at the Alfvén distance. Then, the dimensionless magnetic flux function $\alpha(R, \theta)$ is related to $G(R)$ through the following expression

$$\alpha = \frac{R^2}{G^2(R)}\sin^2\theta. \tag{11}$$

Finally, for homogeneity with the notations in ST94, STT99 and STT02, we have also introduced the function $F(R)$, which is the negative logarithmic derivative of the well known expansion factor used in solar wind theory (Kopp & Holzer 1976):

$$F(R) = 2\left[1 - \frac{\mathrm{d}\ln G(R)}{\mathrm{d}\ln R}\right]. \tag{12}$$

We recall that the value of F defines the shape of the poloidal streamlines. For $F(R) = 0$ the streamlines are radial, for $F(R) > 0$ they are deflected towards the polar axis (with $F = 2$ corresponding to cylindrical collimation) while for $F(R) < 0$ they flare towards the equatorial plane.

2.2. Parameters and variables

The model is controlled by the following four parameters.

- The parameter δ which governs the non spherically symmetric distribution of the density with a linear increase (or decrease) of the density when receding from the rotational axis for $\delta > 0$ ($\delta < 0$);
- the parameter λ which is related to the rotation of the poloidal streamlines at the Alfvén surface $R = 1$;
- the parameter κ which controls the non spherically symmetric distribution of the pressure. For $\kappa < 0$ ($\kappa > 0$) the gas pressure decreases (increases) by moving away from the polar axis. In this paper we confine our attention to overpressured jets, i.e., when $\kappa < 0$;
- the gravitational field is written as

$$\boldsymbol{g} = -\frac{\mathcal{G}\mathcal{M}}{r^2}\hat{r} = -\frac{1}{2}\frac{V_*^2}{r_*}\frac{\nu^2}{R^2}, \tag{13}$$

where $\mathcal{M}$ is the central gravitating mass. As a consequence there is an extra parameter ν which is the ratio of the escape and flow speeds at the Alfvén surface on the polar axis ($R = 1$),

$$\nu^2 = \frac{\mathcal{G}\mathcal{M}}{r_* V_*^2}, \tag{14}$$

With the assumed axisymmetry, the original system of the MHD equations reduces to two coupled partial differential equations for the density and the magnetic flux. Furthermore, with the self-similarity assumption, the components of V and $\boldsymbol{B}$ can be written as functions of θ and three functions of R,

namely $G(R)$, $F(R)$ and $M(R)$. In this way, the momentum conservation law reduces to three ordinary differential equations which together with Eq. (12) can be solved for the four variables $M^2(R)$, $F(R)$, $\Pi(R)$ and $G(R)$ (see Appendix A).

2.3. Efficiency of the magnetic rotator

By integrating the momentum equation along a fieldline we obtain the conserved total energy flux density per unit of mass flux density. This is equal to the sum of the kinetic and gravitational energies, together with the enthalpy and net heating along a specific streamline. In the framework of the present meridionally self-similar model, the variation of the energy across poloidal fieldlines gives an important extra parameter (STT99):

$$\epsilon = \frac{M^4}{(GR)^2}\left[\frac{F^2}{4} - 1\right] - \kappa\frac{M^4}{G^4} - \frac{(\delta - \kappa)\nu^2}{R}$$
$$+ \frac{\lambda^2}{G^2}\left(\frac{M^2 - G^2}{1 - M^2}\right)^2 + 2\lambda^2\frac{1 - G^2}{1 - M^2} \tag{15}$$

which is a constant on <u>all</u> streamlines (ST94).

Physically, ϵ is related to the <u>variation</u> across the fieldlines of the specific energy which is left available to collimate the outflow once the thermal content converted into kinetic energy and into balancing gravity has been subtracted (STT99).

We can express $\epsilon/2\lambda^2$ in terms of the conditions at the source boundary r_0 (see STT99 for details),

$$\frac{\epsilon}{2\lambda^2} = \frac{E_{\mathrm{Poynt.,0}} + E_{\mathrm{R,0}} + \Delta E_{\mathrm{G}}^*}{E_{\mathrm{MR}}}, \tag{16}$$

where E_{MR} is the energy of the magnetic rotator (see Eq. (2.5a) in STT99), $E_{\mathrm{Poynt.,0}}$ is the Poynting energy, E_{R_0} is the rotational energy at the base and ΔE_{G}^* is the excess or deficit on a nonpolar streamline compared to the polar one of the gravitational energy (per unit mass) which is not compensated by the thermal driving,

$$\Delta E_{\mathrm{G}}^* = -\frac{\mathcal{G}\mathcal{M}}{r_0}\left[1 - \frac{T_0(\alpha)}{T_0(\mathrm{pole})}\right] = -\frac{\mathcal{G}\mathcal{M}}{r_0}\frac{(\delta - \kappa)\alpha}{1 + \delta\alpha}. \tag{17}$$

For $\epsilon > 0$ collimation is mainly provided by magnetic means, while for $\epsilon < 0$ the outflow can be confined only by the thermal pressure gradient, something which is not possible for overpressured flows. Accordingly, in STT99 we defined flows with positive or negative ϵ as *Efficient* or *Inefficient* Magnetic Rotators, respectively (**EMR** or **IMR**).

A solution is determined by the four parameters ν, ϵ, κ and λ. The parameter δ can be deduced from the constraint imposed by the integral ϵ, Eq. (15), which has the following expression at the Alfvénic singular surface ($R = 1$):

$$\epsilon = (\kappa - \delta)\nu^2 + \lambda^2\left(\tau^2 + 1\right) - (1 - \kappa) + F_*^2/4, \tag{18}$$

where $\tau[= (2 - F_*)/p]$ is given by Eq. (A.8).

3. Asymptotic behaviour of the solutions

For $R \gg 1$ the asymptotic parameters of collimated outflows ($F_\infty = 2$, G_∞ and M_∞ bounded) depend on the value of ϵ.
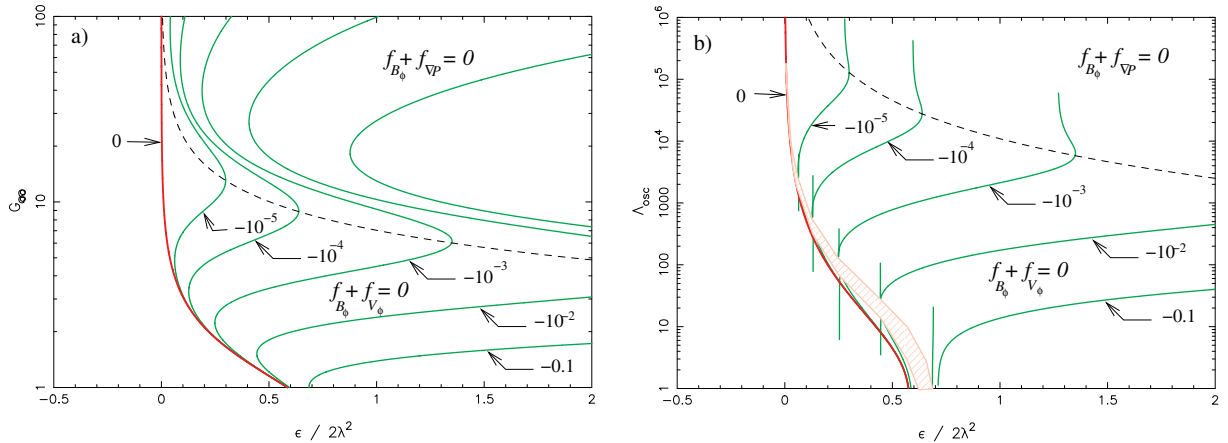
Fig. 1. In **a)** is shown a plot of the dimensionless asymptotic radius of the jet G_∞ and in **b)** of the wavelength of the oscillations $\Lambda_{\mathrm{osc.}}$ in units of r_*/λ, vs. $\epsilon/2\lambda^2$ for a representative value of the terminal pressure, $\Pi_\infty = 0.01$. Each curve is drawn for a constant value of $\kappa/2\lambda^2$ which ranges from -0.1 to -10^{-5}. To the right of the dashed line is the domain of pressure supported and magnetically confined jets ($f_{B_\phi} + f_{\nabla P}$) while to the left of the dashed line is the domain of magnetocentrifugal jets ($f_{B_\phi} + f_{V_\phi}$) (STT99).

Force balance across the poloidal streamlines, $f_{\nabla P} + f_{B_\phi} + f_{V_\phi} = 0$, with $f_{\nabla P}$, f_{B_ϕ} and f_{V_ϕ} the pressure gradient, magnetic stress and centrifugal volumetric force, respectively, calculates M_∞ and G_∞ as functions of the parameters $\epsilon/(2\lambda^2)$, $\kappa/(2\lambda^2)$ and Π_∞.

The asymptotic properties of these self-similar winds have been discussed in detail in STT99, and here we briefly summarize their main features for the case of overpressured outflows ($\kappa < 0$), some of which are displayed in Fig. 1.

- Two main asymptotic regimes exist. In one the outflow is collimated by the pinching of the toroidal magnetic field ($\epsilon > \epsilon_{\mathrm{lim}} > 0$) and in the other the outflow expands radially ($\epsilon < \epsilon_{\mathrm{lim}}$);
- for $\kappa \to 0$ we have collimation for any value of $\epsilon > 0$: there is no pressure gradient across the streamlines and the flow can be supported only by the centrifugal force ($f_{B_\phi} + f_{V_\phi} = 0$);
- magnetically collimated flows are supported either by the centrifugal force or by the thermal pressure. For a given set of values of $\kappa/2\lambda^2$ and Π_∞, solutions with an increasing asymptotic radius G_∞ are found to pass from centrifugally supported to pressure supported. For each regime and a given value of $\epsilon/2\lambda^2$ two solutions are found with a different asymptotic radius G_∞;
- collimated streamlines always show oscillations. This behaviour is consistent with the results found in more general, non self-similar treatments (Vlahakis & Tsinganos 1998) and numerical simulations. However as we move along a given curve with a fixed value of $\kappa/(2\lambda^2)$ and in the direction of increasing G_∞ (see Fig. 1), in the region of centrifugally supported flows, $\epsilon/(2\lambda^2)$ decreases and then increases again. In the region of minimum $\epsilon/(2\lambda^2)$ where the two regimes of centrifugally supported solutions merge we see that the wavelength becomes imaginary. This suggests that in this region cylindrical asymptotics is unstable.

In conclusion and within the present model, from the asymptotic analysis it turns out that overpressured meridionally self-similar outflows from **IMR** should always radially expand with an asymptotically vanishing pressure $\Pi_\infty = 0$. Conversely, outflows from **EMR** should undergo a transition from radially expanding to cylindrically collimating, as the efficiency of the magnetic rotator increases.

4. Numerical results

4.1. Numerical technique

As in STT02, using routines of the NAG scientific package suitable for the treatment of stiff systems and the Runge-Kutta algorithm, Eqs. (A.1)–(A.7) and (12) are integrated upstream and downstream of the vicinity of the Alfvén transition ($R_{\mathrm{in}} = 1 \pm \mathrm{d}R$) with $M_{\mathrm{in}} = 1 \pm p\,\mathrm{d}R$ and $G_{\mathrm{in}} = 1 \pm (2 - F_{\mathrm{in}})\mathrm{d}R$ ($F_{\mathrm{in}} \approx F_*$). The slope p of M at $R = 1$ is given in Eq. (A.8). We first integrate upstream tuning the value of F_{in} until we select the critical solution that smoothly crosses the singularity corresponding to the slow magnetosonic point and reaches the base of the wind R_0 with $M \to 0$. With this value of F_{in} we then integrate downstream to the asymptotic region (with R_∞ usually between 10^4 and 10^6).

Then, if the solution tends to become asymptotically radial or paraboloidal with a non zero pressure, we find that the transverse gradient of the pressure dominates and forces the flow streamlines to eventually flare towards the equator (or the pole if pressure is negative) at a finite distance. Such a solution is terminated. As is well known from the Parker wind theory, a physically acceptable solution which obtains radial asymptotics should satisfy the correct boundary condition at infinity, namely that the pressure should go to zero there. For this reason, we simply tune the value of the pressure Π_{in} ($\approx \Pi_*$) such that $\Pi(R \to \infty)$ vanishes. The various forces acting along and normal to a poloidal streamline are indicated in Figs. 2–4 as follows (see STT02): f_{g}, for the gravitational volumetric force, $f_{V_{\mathrm{p}}}$ for the inertial volumetric force, $f_{B_{\mathrm{p}}}$ for the poloidal magnetic volumetric force, and $f_{\nabla P}$, f_{V_ϕ}, f_{B_ϕ} as defined in Sect. 3.

If an extra critical point appears downstream of the Alfvén transition, we tune the value of Π_{in} ($\approx \Pi_*$) such that the solution crosses this second X-type critical point. After
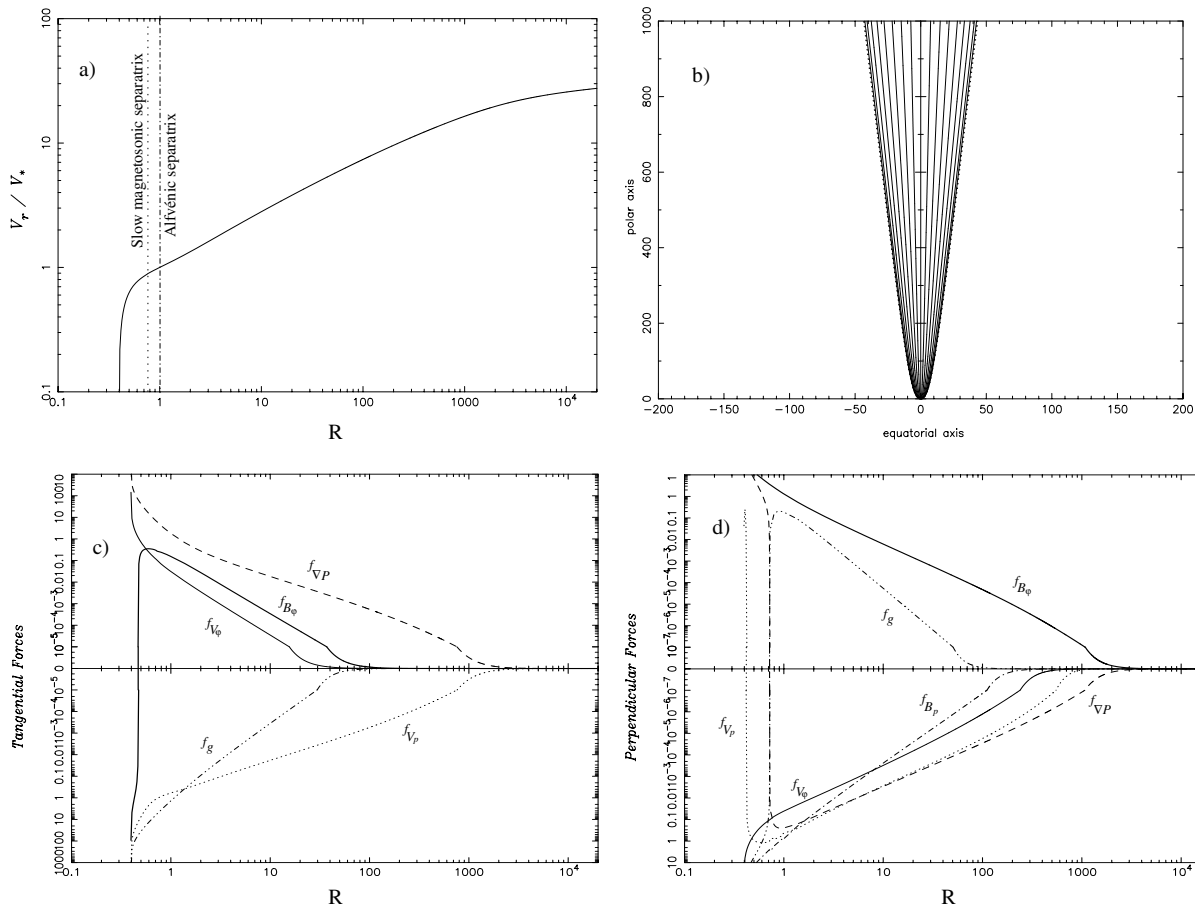
Fig. 2. Typical example of a *radially* expanding solution. In **a)** V_r/V_* along the polar axis is plotted vs. R the radial distance in units of the polar Alfvén radius. The dotted line corresponds to the slow critical point and the dot-dashed one to the Alfvén point. In **b)** the shape of the poloidal streamlines is plotted for $\epsilon/(2\lambda^2) = -0.05$ and $\kappa/(2\lambda^2) = -0.0005$, with the dotted line indicating a streamline which is not connected to the central star but to the surrounding accretion disk. The various volumetric forces acting along and perpendicular to a given streamline are also plotted vs. R in the two lower panels. In **c)** positive forces (*upper half*) acting along the flow are accelerating forces while negative ones (*lower half*) are decelerating ones. The inertial force is negative as it is the opposite of acceleration. In **d)** positive forces (*upper half*) tend to collimate while negative forces (*lower half*) are decollimating. Symbols of the forces are defined in the text.

the critical point the solution is either collimated or terminated. We can always adjust the value P_0 such that the total pressure remains positive everywhere (e.g. Figs. 3 and 4).

Finally, if the solution naturally collimates and does not cross the second critical point, we obtain two alternatives. Either we choose $P_0 = 0$ as in STT99 and tune the value of the pressure Π_{in} ($\approx\Pi_*$) such that $\Pi(R)$ is positive everywhere. Or, we let $P_0 \neq 0$ as in STT02 (e.g. Figs. 4), and choose a value of $P_0 > 0$ such that the total pressure remains positive everywhere.

It is worth to note that for $\kappa < 0$, even though the pressure along the polar axis is always positive, it becomes negative for those nonpolar streamlines which correspond to $\alpha \geq -1/\kappa$, as it happened in TTS97. Thus, conversely to the $\kappa > 0$ collimated solutions analysed in STT02, the present solutions cannot be extended to all streamlines away from the flow axis. This limitation however is expected since is well known that the meridionally self-similar solutions are more adapted to describe the flow close to its axis (cf. ST94) than far from it.

4.2. Behaviour of the solutions with κ and ϵ

In this subsection we have fixed $\nu = 1$ and $\lambda = 1$ (with the value of δ deduced from Eq. (18)) and analysed the trends of the solutions for different values of $\epsilon/2\lambda^2$, $\kappa/2\lambda^2$ and Π_*. Even though this is a rather restricted set which does not exhaust the whole space of the parameters, it may nevertheless illustrate the main characteristics exhibited by the solutions.

For a constant negative value of κ and for ϵ increasing from negative to positive values three types of solutions are successively found. In the $\kappa/2\lambda^2$ vs. $\epsilon/2\lambda^2$ plane of Fig. 5 are sketched the three distinct asymptotic regimes of the outflow:

– *Radial asymptotics solutions*. An example of such a solution is shown in Figs. 2, where we have plotted the dimensionless radial speed along the polar axis vs. the radial distance R, the shape of the poloidal streamlines and the volumetric forces acting along and perpendicular to the flow. Such solutions correspond to the filled squares in the $[\epsilon/2\lambda^2, \kappa/2\lambda^2]$ plane displayed in Fig. 5.
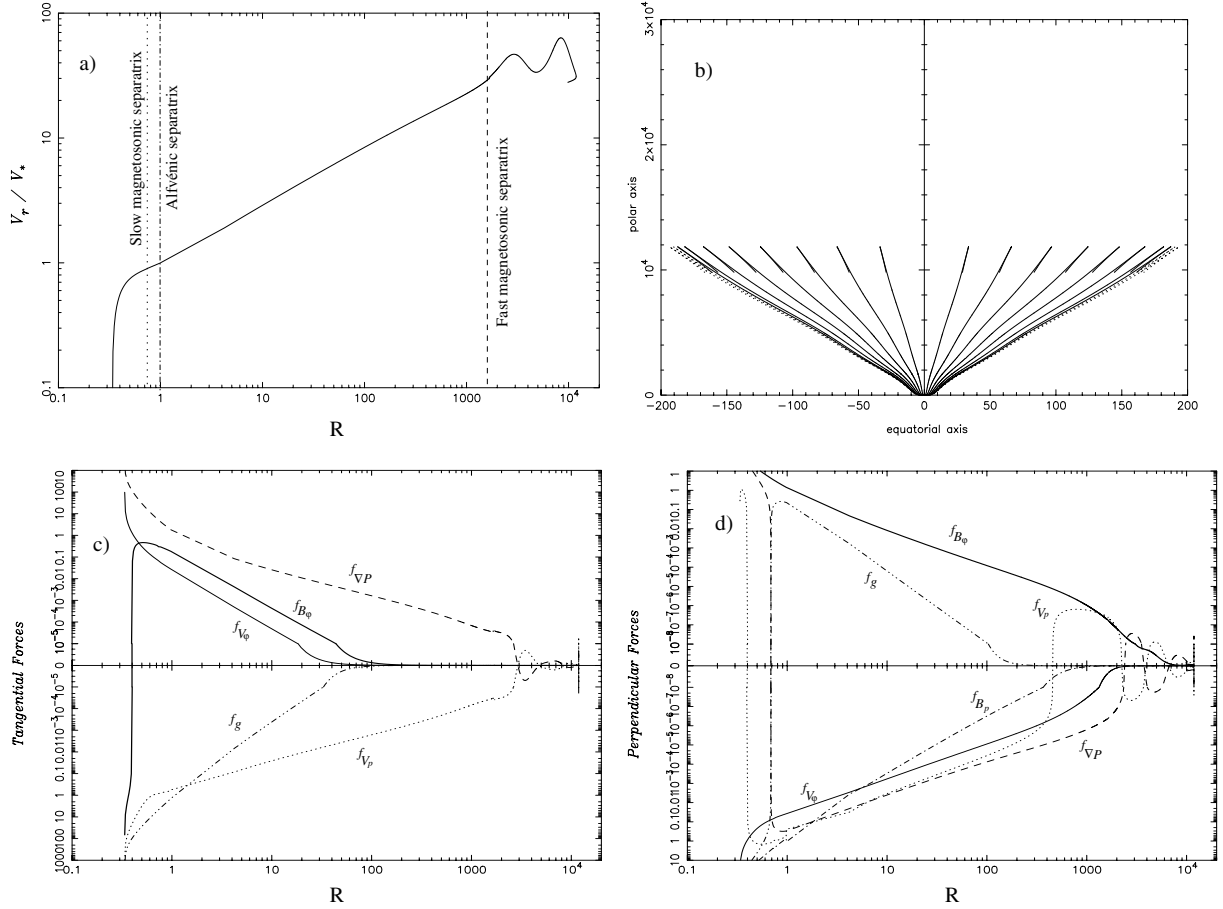
Fig. 3. Typical example of a *terminated* critical solution. The same plots to those of Fig. 2 are shown for $\epsilon/2\lambda^2 = 0.05$ and $\kappa/2\lambda^2 = -0.00015$. In **a)** the dotted line corresponds to slow critical point, the dot-dashed one to the Alfvén point and the dashed line to the fast critical point. Positive forces are accelerating in the upper part of **c)** and collimating in the upper part of **d)**, while negative forces decelerate in **c)** and decollimate in **d)**.

– *Terminated oscillating solutions*, with a typical example shown in Figs. 3. Terminated solutions correspond to the crosses of the $[\epsilon/2\lambda^2, \kappa/2\lambda^2]$ plane (Fig. 5).
– *Cylindrical asymptotics solutions*, with a typical example shown in Figs. 4. Asymptotically cylindrical solutions correspond to the stars of the $[\epsilon/2\lambda^2, \kappa/2\lambda^2]$ plane (Fig. 5).

The same evolutionary trend is found for a given positive value of ϵ by increasing κ from negative values (see Fig. 5). The character of the solutions changes from radial asymptotics to cylindrical ones through a transition where the solutions are terminated.

If $\epsilon < 0$, we are in the regime of IMR and the transverse pressure gradient does not let the flow to cylindrically collimate. In fact, solutions with a nonvanishing pressure are either terminated with negative pressure, or they have excessive flaring ($F = -2$) such that all streamlines close at the equator, a rather unphysical situation as discussed in ST94. A third type of solutions is found when the pressure at the Alfvén surface $\Pi_\star$ is tuned such that Π_∞ vanishes, as we mentioned above. Then, as predicted by the asymptotic analysis, the flow streamlines asymptotically expand radially, with the Alfvén number increasing unboundedly far from the base while the flow speed

is bounded ($V_r \longrightarrow V_0, B_r \longrightarrow R^2, M \longrightarrow R$). For a given ϵ, by decreasing κ to more negative values (Fig. 5), the solutions with radial asymptotics have a decreasing terminal velocity and initial pressure $\Pi_\star$. This can be understood as follows. The transverse pressure gradient is proportional to $\kappa\Pi$, and lower values of $\Pi_\star$ are needed to open the lines radially and at the same time as the flaring is higher the velocity is lower as discussed in Tsinganos & Sauty 1992. This last result is unexpected from polytropic wind theory where a larger flaring leads to larger velocities Kopp & Holzer (1976) but this is precisely what has been observed for the fast component of the solar wind during the minimum and the maximum of the last solar cycles (see Wang 1995; Wang & Sheeley 2003).

For $\epsilon > 0$ and κ lower than some threshold value κ_1, the same behaviour is observed. Solutions with an asymptotically vanishing pressure are radial. Other solutions are either flaring with $F_\infty = -2$ or refocalizing on the axis if the pressure becomes negative and then flaring again with $F_\infty = -2$.

When κ reaches the value κ_1, we have the transition from squares to crosses in Fig. 5. Now a second X-type critical point emerges in the superAlfvénic regime for $R > 1$. Numerically, this second critical point appears at a finite distance and is not coming from infinity upstream, as one would expect. We no-
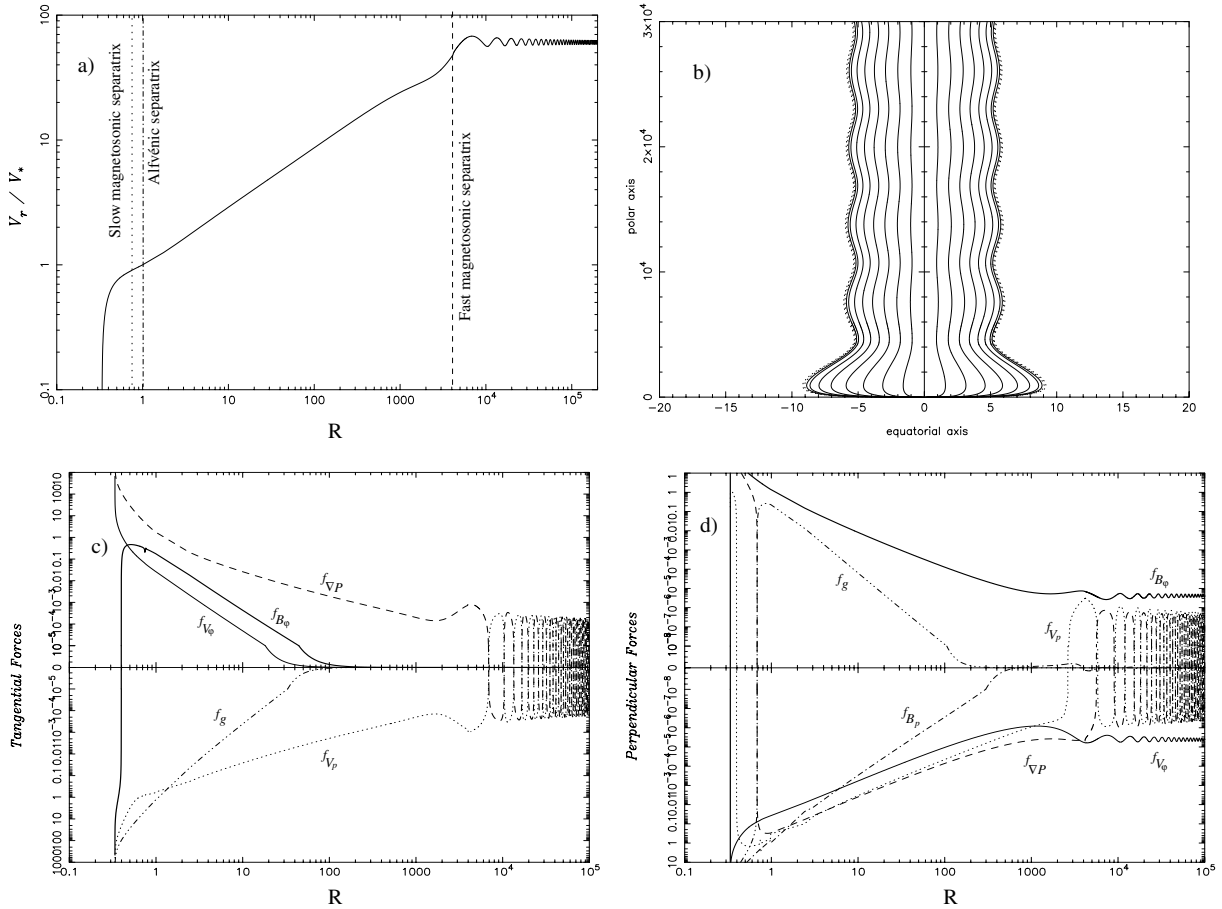
Fig. 4. Typical example of a *collimated* critical solution. The same plots to those of Fig. 2 for $\epsilon/2\lambda^2 = 0.05$ and $\kappa/2\lambda^2 = -0.000005$. In **a)** the dotted line corresponds to the slow critical point (SMSS), the dot-dashed to the Alfvén point and the dashed to the fast critical point (FMSS). Positive forces are accelerating in **c)** (*upper part*) and collimating in **d)** (*upper part*), while negative forces decelerate in **c)** and decollimate in **d)**.

tice further that, assuming $|\kappa| \ll 1$, for radially expanding solutions the quantity R^2/G^2 remains bounded, such that $\mathcal{D}$ does not reverse sign in this case, cf. Eq. (A.4). Conversely if the flow tends to be collimated or becomes radial very slowly the above quantity rapidly increases with R for $R \gg 1$, leading to the appearance of this new singularity [$\mathcal{D} = 0$ in Eq. (A.4)]. This explains the emergence of the second critical point in such cases.

For a given range of κ-values, $[\kappa_1, \kappa_2]$, the two unphysical families which flare with $F_\infty = -2$ separate at a finite distance. In principle the only possible solution would be the critical one that crosses this new X-type critical point. However, it turns out that this critical solution always shows downwind of the position of the critical point oscillations of increasing amplitude and eventually terminates in a loop at a finite distance. The termination position gets closer to the critical point by further increasing κ to less negative values and/or increasing ϵ. This type of solutions may be physically unacceptable since they do not extend up to infinity, unless they are terminated by a shock, with a positive pressure (we discuss this point in more detail in the next paragraph). In this case, this extra critical point seems to be the first of two or more fast critical transitions which seem to appear in the Weber & Davis 1967 1-D solutions topologies and also in the 2-D analysis of Heyvaerts & Norman 1989. Similarly to those examples, the solutions loop back rather sharply, returning upstream (Fig. 3).

If the efficiency of the magnetic rotator increases further and/or κ gets larger than κ_2, then a new family of cylindrically collimated solutions enters the picture. Topologically, they appear once the turning point of the terminated solutions reaches the X-type critical point. They have the typical properties of those from an **EMR** with $\kappa > 0$ (see STT02). The critical solution itself changes as it becomes also cylindrically collimated.

The various families of solutions which exist in that case are as follows. First, with rather high pressures we have solutions which still flare with $F_\infty = -2$. Second, with rather low pressures we have the solutions which loop back. And finally, in between those two families of solutions, for a given intermediate range of Π_*, we have the third family of cylindrically collimated ones.

One member of this third family of solutions crosses the X-type singularity which is still present at the border between cylindrical and looping solutions. The other members of this third family of solutions are noncritical. The critical solution is analogous to the limiting solution of STT02 for $\kappa > 0$.
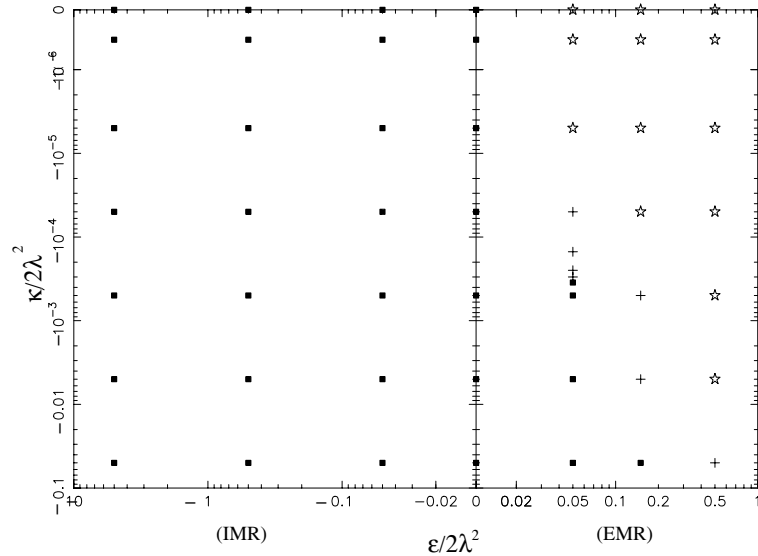
Fig. 5. Regions of the radially expanding (full squares), terminated (crosses) and collimated solutions (stars) in the plane of $\epsilon/2\lambda^2$ and $\kappa/2\lambda^2$.

Furthermore we know from the asymptotic analysis that different branches of solutions are present, corresponding to centrifugally or pressure supported flows. The present numerical results show that only the configuration with the smallest transversal radius can be attained by the jet, which is supported by the centrifugal force. Thus, as predicted by the asymptotic analysis performed in STT99, all cylindrically collimated solutions including the critical ones have almost the same asymptotic behaviour. In other words the pressure plays a minor role in achieving the asymptotic configuration of these solutions.

5. Properties of the critical solutions

5.1. Cylindrically collimated solutions

An interesting novel feature in the present cylindrically collimated solutions is the appearance of two X-type critical points within the flow domain, in addition to the Alfvén critical point. The only other known case where a unique steady MHD outflow solution is filtered by three critical points is the case of a radially self-similar solution (Vlahakis et al. 2000; Ferreira & Casse 2004). In general, at such critical points the bulk flow speed equals to one of the characteristic speeds in the problem. Hence, it is of physical interest to associate the flow speeds at these critical X-type points to some characteristic MHD speeds. In that connection, we first note that the present solutions posses the symmetries of meridional self-similarity and axial symmetry. Thus, in spherical coordinates (r, θ, φ), the self-similarity direction is $\hat{\theta}$ and the axisymmetry direction is $\hat{\varphi}$. Therefore, a wave that preserves those two symmetries should propagate along the $\hat{r}$-direction in the meridional plane. *First*, the incompressible Alfvén mode propagates along the magnetic field ($\boldsymbol{B}$) with velocity V_a and in the direction $\hat{r}$ of the poloidal plane with a phase speed $V_{a,r} = \boldsymbol{B} \cdot \hat{r}/\sqrt{4\pi\rho}$. Thus, at the Alfvén point we should have $M = 1$. And *second*, the compressible slow/fast MHD modes propagate in the direction $\hat{r}$

with a phase speed $V_X \equiv V_{\text{slow},r}$, or, $V_X \equiv V_{\text{fast},r}$ which satisfy the quartic

$$V_X^4 - V_X^2 \left(V_a^2 + C_s^2\right) + C_s^2 V_{a,r}^2 = 0. \tag{19}$$

Hence, when the above equation is satisfied the governing Eqs. (A.1)–(A.3) have X-type singularities and $V_X = V_p \cdot \hat{r}$.

On the other hand, it is well known that in the MHD flow system there exist two hyperbolic regimes wherein characteristics exist: the inner, which is bounded by the cusp and the slow magnetosonic surfaces and the outer extending downstream of the fast magnetosonic point. Within each of those two hyperbolic regimes, there exists one limiting characteristic or separatrix surface: the slow magneto-acoustic separatrix surface (SMSS) inside the inner hyperbolic regime and the fast magneto-acoustic separatrix surface (FMSS) inside the outer hyperbolic regime (Bogovalov 1994; Tsinganos et al. 1996). The true critical points are precisely found on these two separatrices. For example, in the case presented in Figs. 4, the SMSS is at $R = 0.751$ while the FMSS is located at $R = 4150$.

In the underpressured solutions studied in STT02 we have found only the X-type critical point inside the inner hyperbolic regime wherein the radial outflow speed is $V_r = V_{\text{slow},r}$ (ST94). Now, in the regime of cylindrically collimated solutions (domain with stars in Fig. 5), there exists a unique critical solution that also crosses the second critical point. This solution always has negative values of $\Pi(R)$ asymptotically. Thus, in order to have positive values of the total pressure everywhere in the flow, we have to adjust P_0 to some positive value (Eq. (9)). The closer to zero is κ the more negative becomes the function Π and the larger is the minimum value needed for P_0.

The fast magnetosonic nature of this second critical point can be analysed by drawing the characteristics in the vicinity of this separatrix critical surface, provided that we are able to define there the sound speed. Although the sound speed is ill-defined in our model, we can nevertheless deduce its
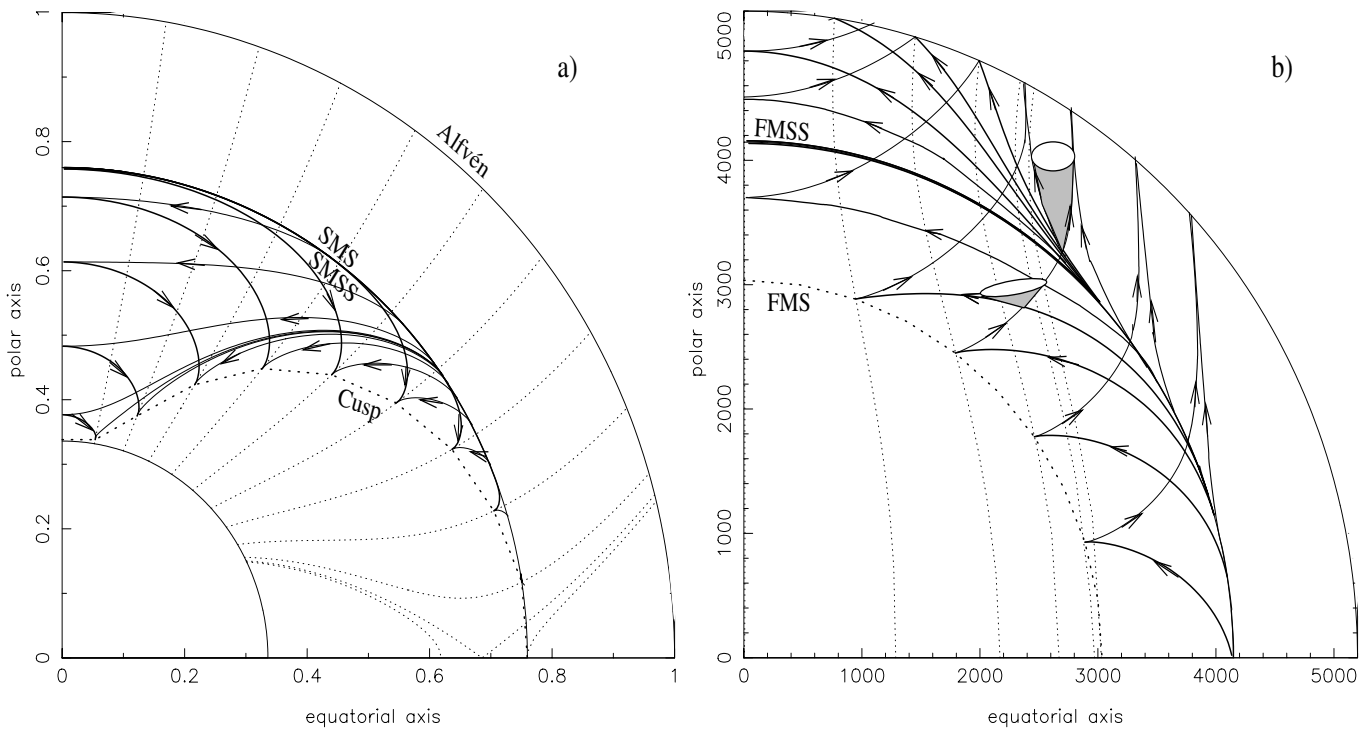
Fig. 6. Slopes of the two families of characteristics of the collimated critical solution of Figs. 4 in each of the two hyperbolic regimes of the problem. In **a)** the slow magnetoacoustic separatrix surface (SMSS) is at $R = 0.751$ just before the slow magnetoacoustic surface (SMS). In **b)** the fast magnetoacoustic separatrix surface (FMSS) is at $R = 4158$ above the fast magnetoacoustic surface (FMS) at about $R = 3000$. Arrows indicate the direction of MHD signal propagation while two Mach cones above and below the FMSS are also shown.

value at the critical surface by following the steps presented in Tsinganos et al. 1996,

$$C_s^2 = \left.\frac{\partial P}{\partial \rho}\right|_{(R,\alpha)} \qquad (20)$$

$$= -\left.\frac{V_\star^2}{2}\frac{\partial \Pi\left(M^2, R\right)}{\partial M^2}\right|_{(R,\alpha)} M^4 \frac{1 + \kappa\alpha}{1 + \delta\alpha} + H(R, \alpha), \qquad (21)$$

with $H(R, \alpha)$ a function which becomes zero at the critical surface. The condition at the critical point is equivalent to setting equal to zero the denominator [Eq. (A.4)] of Eqs. (A.2) and (A.3),

$$\left(M_a^2 - 1\right)\left(1 + \kappa\frac{R^2}{G^2}\right) + \frac{F^2}{4} + R^2\lambda^2\frac{\left(1 - G^2\right)^2}{\left(1 - M_a^2\right)^2} = 0. \qquad (22)$$

Together with the previous definition of the sound speed and Eq. (A.1), this can then be put into the form of Eq. (19) with $V_X = V_r$.

Moreover assuming that $H(R) = 0$ in all space we can calculate the slopes of the two characteritics in the regions where the equations are hyperbolic. The results are displayed in Figs. 6 for the cylindrically collimated solution of Figs. 4. We show that there is an inner hyperbolic domain bounded downstream by the slow magnetosonic transition as well as an outer hyperbolic domain bounded upstream by the fast magnetosonic surface. As in Tsinganos et al. 1996, the transition from hyperbolic to elliptic in Fig. 6a is very close to the critical transition SMSS such that it is impossible to distinguish between the

two without zooming closer than what is done in this figure. Instead in Fig. 6b, the FMSS is clearly distinguishable from the FMS. Thus, in both cases the magneto-acoustic separatrices clearly differ from the corresponding magneto-acoustic transitions in the same way the ergosphere differs from the event horizon of a rotating black hole (see Sauty et al. 2002b).

5.2. Terminated solutions

We have seen that the main feature of the terminated solutions is the onset, downstream of the FMSS, of oscillations with growing amplitude. This is likely to be related to some instability that does affect the configuration of the outflow which thus cannot attain any steady configuration. This is confirmed by the perturbative analysis in STT99: for this set of parameters the asymptotic solutions show a turning point (see Fig. 1, left panel, and Figs. 1 in STT99) and in this region the typical oscillations of the asymptotic streamlines are not present, namely their wavelengths become imaginary (see Fig. 1, right panel, and Fig. 8, Eqs. (5.4)–(5.5) in STT99).

The cylindrical solutions with the second critical point are extended to infinity because there is some freedom on Π_∞. For the terminated solutions, cylindrical asymptots are forbidden because the cylindrical regime is unstable (infinite wavelength of the oscillations). The only remaining solution is for the lines to become radial. However, by crossing the second critical point the value of Π is fixed, so there is little chance that the solution becomes radial or paraboloidal because the pressure does not vanish asymptotically. By plotting the forces

across the lines, we see that in fact at the turning point the pressure gradient dominates. It is balanced only by the curvature force of the poloidal velocity which creates the turning point and the termination of the solution.

5.3. Radial solutions

In outflows which are launched dominantly thermally (cf. Fig. 2c), the streamlines start with a basically radial shape close to their base. Further away, if the outflow is strongly overpressured ($\kappa < \kappa_1$), the asymptotics remains radial. Hence, there is no drastic change in the geometry of the streamlines. On the other hand, in mildly overpressured ouflows ($\kappa > \kappa_2$), the asymptotics changes to cylindrical (in the intermediate case $\kappa_1 < \kappa < \kappa_2$ the oscillations are so strong that the solution terminates). Thus, for $\kappa > \kappa_2$, there exists a transition region between the base and the asymptotic regime wherein the cylindrical geometry is finally obtained after the basal roughly radial regime. During that transition phase the outflow naturally passes from a stage of oscillations in its radius, Mach number and other physical parameters. These oscillations can be understood as the result of the interplay of the pinching magnetic tension force and the resulting reaction by the flow (conservation of angular momentum). In consistency with the previous explanation, a conspicuous feature appearing in the asymptotically radially solutions is the lack of any oscillation of the poloidal streamlines, a result confirming the physical origin of these oscillations.

In that connection, theoretical arguments and various analytical self-similar solutions have shown that a notable common feature of all self-consistent, self-similar MHD solutions which become finally cylindrically collimated is that the outflow passes from a stage of oscillations in its physical parameters (Vlahakis & Tsinganos 1997). Such oscillatory behavior of collimated outflows is not restricted to the few specific models examined so far, but instead it seems to be a rather general physical property of an MHD outflow which starts noncylindrically before it reaches collimation. Note that the same feature of oscillations has been also found in non-self-similar simulations of outflows which start radially before the magnetic tension converts them to a cylindrical shape (Tsinganos et al. 2003).

6. Conclusions

6.1. Summary of results

In this paper we continued the analysis of Meridional Self-Similar Models (MSSM, hereafter) by confining our attention to the study of outflows with a density increasing away from the axis and towards the surrounding streamlines [cf. Eq. (8) with $\delta > 0$] and with a pressure decreasing from the axis [cf. Eq. (9) with $\kappa < 0$]. In such *overpressured* outflows with a central dip in the density distribution, the temperature is strongly peaked at the axis relatively to the surrounding regions, more than in the *underpressured* outflows studied in STT02.

We have been able to construct solutions describing outflows starting subsonically and subAlfvénically from the central gravitating source and its surrounding accretion disk and, after crossing the MHD critical points, reaching high values of the Alfvén Mach number.

In terms of asymptotic profiles three broad types of solutions are found:

- (a) Collimated jet-type outflows from **EMR** where the outflow is confined by the magnetic hoop stress, provided that they are not too overpressured (κ not too negative, i.e., $\kappa > \kappa_2$). Among those solutions, a unique one crosses three critical points: the SMSS, the Alfvén and the FMSS. We analysed those solutions and have shown that the separatrices indeed correspond to the three familiar separatrices in MHD wind theory. This class of critical solutions exhibits at large distances oscillations between over- and under-pressured flow (Figs. 4).
- (b) Radially expanding wind-type outflows, analogous to the solar wind, for all **IMR** [cf. Eq. (15) with $\epsilon < 0$] or strongly overpressured sources from **EMR** ($\epsilon > 0$, $\kappa < \kappa_1$). Those solutions cross the slow and the Alfvén point and the initial pressure is fixed by the outer boundary condition that the terminal pressure should become zero. They do not show any intermediate topology of a third critical point.
- (c) Terminated solutions. Such solutions cross again the three MHD separatrices. The onset of the increasing amplitude oscillations and the termination of the solutions can be understood because cylindrical asymptotics were shown to be unstable. As for disk wind solutions crossing all critical points, shown in Vlahakis et al. 2000, such terminated solutions can support terminal shocks. This is the opposite of the solutions of refocalizing disk wind usually used in models (e.g., Ferro-Fontán & Gómez de Castro 2003). Nevertheless, our terminated solutions are usually having very high temperature in the far regime and thus they are unphysical.

Although from the asymptotic analysis presented in STT99 we could not exclude the existence of paraboloidal asymptotics, we could not find numerically any such solution except in the limiting case $\epsilon = \kappa = 0$ (ST94). We conjecture that these paraboloidal solutions could be found in principle in the transition region between radial and cylindrical asymptotics. However steady equilibrium is impossible in this region and the solutions terminate before reaching their asymptotic regime.

6.2. Astrophysical implications

Possibly related to the previous discussion on the lack of paraboloidal solutions, we note that, conversely to underpressured jets studied in STT02, the transition of collimated jets to uncollimated winds is not continuous in the parametric space showing a gap where stationnary solutions do not exist. We are tempted to conjecture, then, for some jets with strong transient events, such as violent outbursts, the following scenario: if the outflow configuration is at the interface of the regime with collimated and non collimated solutions, an outburst could be associated with the flip over between the two different classes of asymptotically collimated and radial solutions.

One of the major outstanding questions in astrophysical jets research is how they are generated. Take for example the case of the closer and thus better resolved jets associated with young stellar objects. In that connection one may say that through a combination of observations and numerical simulations we do know several details about the propagation of these jets in the parent cloud and their interaction with their environment but we know relatively fewer details about their generation at the "central engine" (cf. Hartigan 2003; Ray & Bacciotti 2003). At the same time various studies have shown that a high degree of collimation is already achieved very close to the source, namely at 10 to 20 AU (Woitas et al. 2002).

In that content, two wide classes of models are available today to study analytically the launching and eventual collimation of MHD outflows (Vlahakis & Tsinganos 1998); *first*, the family of the so-called radially self-similar models (RSSM) which have as their prototype the Blandford & Payne (1982) model and *second* the family of the so-called meridionally self-similar models (MSSM) which have as their prototype the Sauty & Tsinganos (1994) model and which we have explored in this series of papers. A third class of models are the so-called X-wind models where mass loss originates at a fan of concentrated magnetic flux in the inner disk radius (Shu et al. 1994; Shang et al. 2002).

In an analytical MHD treatment of the problem of outflow launching and subsequent collimation, in the RSSM the driving force and collimation mechanism are basically *magnetic*. Among the limitations of the RSSM is that they are invalid close to the jet axis where they have singularities and are thus more appropriate to describe disk-winds which collimate within several AU from the star (Ferreira 1997; henceforth F97). Also, after several Alfvén radii when the streamlines reach their maximum cylindrical radius, they slowly refocus towards the axis and the solutions terminate. Another difficulty of the cold plasma RSSM is that they predict rather large terminal speeds and too low densities and ionisation fractions and do not accomodate some efficient heating mechanism which is needed in order to explain the observed emission (Dougados 2003). However, Casse & Ferreira (2000) have shown that by including a hot corona above the disk it would help to increase the mass loss rate and thus the terminal densities. In any case, the RSSM deal consistently with the accretion ejection problem and have been recently used with some success to compare observed jet widths and collimation scales in several T Tauri microjets for which we currently have the corresponding observations (Dougados et al. 2000; Pesenti et al. 2003).

On the other hand, in the MSSM for jet acceleration and collimation the driving force is a combination of thermal and magnetocentrifugal terms while collimation can be also achieved by a combination of pressure gradients and magnetic tension forces. In the MSSM however, if the source region of the outflow is restricted to be only the stellar base, the resulting mass loss is unrealistically low, unless it includes the inner part of the disk. Nevertheless, an interesting fact is that observations clearly show that jets extend to relatively great distances (100 to 1000 AU) from the protostar where the observation of forbidden line emission means that the jets are still warm/hot at such large distances. But then if jets are launched from small regions and also expand, they should cool adiabatically. The question arises then on how do these jets remain hot at such distances from the protostar. Clearly a heating mechanism is needed. Hence, observations seem to suggest that thermal gradients, which may originate in a stellar or an accretion heated disk-corona, play an important role in accelerating the flow (Dougados 2003). Such a heating is a basic ingredient of the MSSM and may thus explain the puzzle. In addition steady MSSM stay tightly collimated to unlimited distances from the source without a need to refocus towards their axis in which they are valid without any singularity. Furthermore, it has been suggested that HH jets may be the progenitors of the (uncollimated) solar wind outflow, a form in which jets eventually evolve after the star looses angular momentum becoming an inefficient magnetic rotator (ST94, STT99, STT02 and this paper).

However, recent numerical simulations of magnetocentrifugally collimated outflows from a rotating central object and/or a Keplerian accretion disk have shown that relatively low mass and magnetic fluxes reside in the produced jet as compared to the surrounding wind (Tsinganos & Bogovalov 2002; Matt et al. 2003). This is also the case in the solutions presented in ST94 and STT02. In ST94 it is pointed that a significant fraction of the total mass loss rate of the jet is originating in the disk. Observations however indicate that in jets from young stellar objects, the collimated outflow carries higher fluxes than these studies predict. As a solution to this problem it has been proposed that jets may be described as a two-component system composed of an outflow originating at a central object which is surrounded by a disk-wind (ST94, Koide et al. 1998; STT02, Tsinganos & Bogovalov 2002). In that respect, Hartigan et al. 1995 have identified an outer low velocity component (LVC) with velocities in the range of 10 to 50 km s^{-1} along with a high velocity component (HVC) with radial velocities of a few hundred km s^{-1}. According to Kwan & Tademaru (1995) the LVC is probably a low-velocity disk-wind that encompasses the jet. This view was confirmed later by Bacciotti et al. (2002) using HST/STI data to investigate the velocity structure of the DG Tau jet. They found that the kinematics follows an "onion-like" structure with HVC closer to the jet axis and a LVC spread out wider.

Double component jets also clearly appear in time dependent simulations of jets around black holes and stars (e.g., Kudoh et al. 1998; Koide et al. 1998). The magnetic field does not penetrate the black hole magnetosphere, thus the inner plasma is compressed and a pressure driven outflow develops. The surrounding wind is centrifugally driven from the disk and magnetically collimated. However the main difference between double jet component simulations and the present analytical solutions is that the first describe dense core jets while the second model hollow jets. At this point note that both analytical (Hanasz et al. 2000) and numerical (Kudoh et al. 2002) studies of the flow stability tend to show that the inner flow is probably more stable than the Keplerian outer part and this is particularly true in the case of hollow jets. Further comparison of simulations and our analytical modelling is however difficult

because the boundary conditions generally used in disk winds are rather different from the self-similar assumptions used here.

In accordance with the above theoretical and observational difficulties encountered by the single-component models, we propose that jets may indeed be described as a two-component outflow system. The model presented in this paper and in STT02 is by itself a double component jet structure for cylindrically collimated solutions. One part of the jet comes from the star itself. The other comes from the inner boundary of the disk which is connected with the stellar magnetosphere. Such double structure can be applied directly to model jets from T Tauri stars with low mass accretion rate, like RY Tau for instance. However for T Tauri stars having higher mass accretion rate, like DG Tau, a consistent model would be one with an inner outflow described by a ST94-type MSSM, surrounded by a wider F97-type RSSM disk-wind part. For example, in the present MSSM the velocity is peaked at the axis and the degree of collimation increases with velocity, as observed.

Supporting evidence for the previous scenarios comes from recent findings on the rotation of jets from T Tauri stars with high accretion rate, by using either near-infrared long-slit spectroscopy in a series of distant knots (several 1000 AU away), or, by using HST/STIS observations much closer (within 100 AU) (Bacciotti et al. 2002; Coffey et al. 2003). Remarkable fact is that the magnitude of the only recently inferred toroidal velocity in the jets (5–15 km s^{-1} at distances of 20 to 30 AU from the flow axis and at around 100 AU from the plane of the disk) is precisely what some time ago was already inferred from MHD jet launching models (see for example, Tsinganos & Trussoni 1991, Fig. 6; and Tsinganos et al. 1992, Figs. 2, 3 for a MSSM; or, Vlahakis et al. 2000, Figs. 5, 7 for a RSSM). It should be interesting then to further discuss new observations in the context of the two analytical available models (MSSM and RSSM).

Appendix A: MHD equations for meridionally self-similar flows

Under the assumptions of axisymmetry and meridional self-similarity, the MHD equations reduce to the following three ordinary differential equations for $\Pi(R)$, $M^2(R)$ and $F(R)$:

$$\frac{d\Pi}{dR} = -\frac{2}{G^4}\left[\frac{dM^2}{dR} + \frac{M^2}{R^2}(F-2)\right] - \frac{\nu^2}{M^2 R^2}, \tag{A.1}$$

$$\frac{dF(R)}{dR} = \frac{\mathcal{N}_F\left(R, G, F, M^2, \Pi; \kappa, \delta, \nu, \lambda\right)}{R\,\mathcal{D}\left(R, G, F, M^2; \kappa, \lambda\right)}, \tag{A.2}$$

$$\frac{dM^2(R)}{dR} = \frac{\mathcal{N}_M\left(R, G, F, M^2, \Pi; \kappa, \delta, \nu, \lambda\right)}{R\,\mathcal{D}\left(R, G, F, M^2; \kappa, \lambda\right)}, \tag{A.3}$$

where we have defined:

$$\mathcal{D} = \left(M^2 - 1\right)\left(1 + \kappa\frac{R^2}{G^2}\right) + \frac{F^2}{4} + R^2\lambda^2\frac{N_B^2}{D^2}, \tag{A.4}$$

$$\begin{aligned}
\mathcal{N}_F =\ & -(\delta - \kappa)\nu^2\frac{RG^2}{2M^2}F \\
& + \left[2\kappa\Pi G^2 R^2 + (F+1)(F-2)\right] \\
& \times\left(1 + \kappa\frac{R^2}{G^2} - \frac{F^2}{4} - R^2\lambda^2\frac{N_B^2}{D^3}\right) \\
& + \frac{M^2 F}{4}(F-2)\left(F + 2 + 2\kappa\frac{R^2}{G^2} + 2R^2\lambda^2\frac{N_B^2}{D^3}\right) \\
& - \lambda^2 R^2 F(F-2)\frac{N_B}{D^2} \\
& + \lambda^2 R^2\left(1 + \kappa\frac{R^2}{G^2} - R^2\lambda^2\frac{N_B^2}{D^3} - \frac{F}{2}\right) \\
& \times\left(4\frac{N_B^2}{D^2} - \frac{2}{M^2}\frac{N_V^2}{D^2}\right),
\end{aligned} \tag{A.5}$$

$$\begin{aligned}
\mathcal{N}_M =\ & (\delta - \kappa)\nu^2\frac{RG^2}{2M^2}\left(M^2 - 1\right) \\
& + \kappa\Pi R^2 G^2 M^2\frac{F}{2} - \frac{M^4}{4}(F-2)\left(4\kappa\frac{R^2}{G^2} + F + 4\right) \\
& + \frac{M^2}{8}(F-2)\left(8\kappa\frac{R^2}{G^2} + F^2 + 4F + 8\right) \\
& - \lambda^2 R^2(F-2)\frac{N_B}{D} \\
& + \lambda^2 R^2\left(2M^2 + F - 2\right)\left(\frac{N_B^2}{D^2} - \frac{1}{2M^2}\frac{N_V^2}{D^2}\right),
\end{aligned} \tag{A.6}$$

with

$$N_B = 1 - G^2, \quad N_V = M^2 - G^2, \quad D = 1 - M^2. \tag{A.7}$$

The definitions of the various parameters is discussed in Sect. 2.

At the Alfvén radius, the slope of $M^2(R = 1)$ is $p = (2 - F_*)/\tau$, where τ is a solution of the third degree polynomial:

$$\tau^3 + 2\tau^2 + \left(\frac{\kappa\Pi_*}{\lambda^2} + \frac{F_*^2 - 4}{4\lambda^2} - 1\right)\tau + \frac{(F_* - 2)F_*}{2\lambda^2} = 0, \tag{A.8}$$

and the star indicates values at $R = 1$ (for details see ST94).

References

Bacciotti, F., Ray, T. P., Mundt, R., Eisloffel, J., & Solf, J. 2002, ApJ, 576, 222
Blandford, R. D., & Payne, D. G. 1982, MNRAS, 199, 883
Bogovalov, S., & Tsinganos, K. 1999, A&A, 305, 211
Bogovalov, S. 1994, MNRAS, 270, 721
Casse, F., & Ferreira, J. 2000, A&A, 361, 1178
Casse, F., & Keppens, R. 2004, ApJ, 601, 90

Coffey, D., Woitas, J., Bacciotti, F., Ray, T. P., & Eisloffel, J. 2003, in Star Formation at High Angular Resolution, IAU Symp., 221, 284

Dougados, C., Cabrit, S., Lavalley, C., & Menard, F. 2000, A&A, 357, L61

Dougados, C. 2003, in Magnetism and Activity of the Sun and Stars, ed. J. Arnaud, & N. Meunier (EAS Publication Series), 9, 297

Davis, C. J., Berndsen, A., Smith, M. D., Chrysostomou, A., & Hobson, J. 2000, MNRAS, 314, 241

Ferreira, J. 1997, A&A, 317, 340 (F97)

Ferreira, J., & Casse, F. 2004, ApJ, 601, L139

Ferro-Fontán, C., & Gómez de Castro, A. I. 2003, MNRAS, 342, 427

Hanasz, M., Sol, H., & Sauty, C. 2000, MNRAS, 316, 494

Hartigan, P. 2003, Rev. Mex. Astron. Astrofis. (SC), 15, 112

Hartigan, P., Edwards, S., & Ghandour, L. 1995, ApJ, 452, 736

Heyvaerts, J., & Norman, C. A. 1989, ApJ, 347, 1055

Keppens, R., & Goedbloed, J. P. 2000, ApJ, 530, 1036

Kopp, R. A., & Holzer, T. E. 1976, Sol. Phys., 49, 43

Koide, S., Shibata, K., & Kudoh, T. 1998, ApJ, 508, 186

Koide, S., Meier, D. L., Shibata, K., & Kudoh, T. 2000, ApJ, 536, 668

Koide, S. 2003, Phys. Rev. D, 67, 104010-1

Krasnopolsky, R., Li, Z.-Y., & Blandford, R. 1999, ApJ, 526, 631

Krasnopolsky, R., Li, Z.-Y., & Blandford, R. 2003, ApJ, 595, 631

Kudoh, T., Matsumoto, R., & Shibata, K. 1998, ApJ, 508, 186

Kudoh, T., Matsumoto, R., & Shibata, K. 2002, PASJ, 54, 121

Kwan, J., & Tademaru, E. 1995, ApJ, 454, 382

Lima, J. J. G., Sauty, C., Iro, N., Priest, E. R., & Tsinganos, K. 2001b, in Proceedings of the Solar Encounter: The First Solar Orbiter Workshop, ESA SP-493, 269

Matt, S., Winglee, R., & Böhm, K.-H. 2003, MNRAS, 345, 660

Meliani, Z. 2001, rapport de stage de DEA, Master Sc. degree, Université Paris 7

Ouyed, R., & Pudritz, R. E. 1997, ApJ, 482, 712

Pesenti, N., Dougados, C., Cabrit, S., et al. 2003, A&A, 410, 155

Ray, T. P., & Bacciotti, F. 2003, Rev. Mex. Astron. Astrofis. (SC), 15, 106

Sauty, C., & Tsinganos, K. 1994, A&A, 287, 893 (ST94)

Sauty, C., Tsinganos, K., & Trussoni, E. 1999, A&A, 348, 327 (STT99)

Sauty, C., Tsinganos, K., & Trussoni, E. 2002a, A&A, 389, 1068 (STT02)

Sauty, C., Tsinganos, K., & Trussoni, E. 2002b, in Relativistic flows in astrophysics, Lecture Notes in Physics, ed. A. W. Guthmann et al. (Heidelberg: Springer-Verlag), 589, 41

Sauty, C., Tsinganos, K., Trussoni, E., & Meliani, Z. 2003, in The Unsolved Universe: Challenges for the Future, Proc. of JENAM2002, Workshop Jets (Kluwer), in press

Shang, H., Glassgold, A. E., Shu, F. H., & Lizano, S. 2002, ApJ, 564, 853

Shu, F. H., Najita, J., Ostriker, E., et al. 1994, ApJ, 429, 781

Trussoni, E., Tsinganos, K., & Sauty, C. 1997, A&A, 325, 1099 (TTS97)

Tsinganos, K., & Bogovalov, S. 2002, MNRAS, 337, 553

Tsinganos, K., & Sauty, C. 1992, A&A, 255, 405

Tsinganos, K., & Trussoni, E. 1991, A&A, 249, 156

Tsinganos, K., Trussoni, E., & Sauty, C. 1992, in The Sun: A Laboratory for Astrophysics, ed. J. Brown, & J. Schmelz (Kluwer Academic), 349

Tsinganos, K., Sauty, C., Surlantzis, G., Trussoni, E., & Contopoulos, J. 1996, MNRAS, 283, 111

Tsinganos, K., Vlahakis, N., Bogovalov, S., et al. 2003, in The Unsolved Universe: Challenges for the Future, Proc. of JENAM2002, Workshop Jets (Kluwer), in press

Ustyugova, G. V., Lovelace, R. V. E., Romanova, M. M., Li, H., & Colgate, S. A. 2000, ApJ, 541, L21

Vlahakis, N., & Tsinganos, K. 1997, MNRAS, 297, 591

Vlahakis, N., & Tsinganos, K. 1998, MNRAS, 298, 777

Vlahakis, N., Tsinganos, K., Sauty, C., & Trussoni, E. 2000, MNRAS, 318, 417

Weber, E. J., & Davis, L. J. 1967, ApJ, 148, 217

Wang, Y.-M. 1995, ApJ, 449, L157

Wang, Y.-M., & Sheeley, N. R. 2003, ApJ, 587, 818

Woitas, J., Ray, T. P., Bacciotti, F., Davis, C. J., & Eisloffel, J. 2002, ApJ, 580, 336